Rare-Earth Glass Reference Materials for Near Infrared Spectrometry: Correcting and Exploiting Temperature Dependencies

Steven J. Choquette, Lindsey O'Neal, and David L. Duewer*
Analytical Chemistry Division
Chemical Science and Technology Laboratory
National Institute of Standards and Technology
Gaithersburg, MD 20899-8394

*Corresponding Author: David Lee Duewer
NIST
100 Bureau Drive, Stop 8394
Gaithersburg, MD 20899-8394
Tel: 301-975-3935
Fax: 301-977-0685
Eml: david.duewer@nist.gov

ABSTRACT

Quantitative descriptions of the location of seven near infrared (NIR) absorption bands as functions of temperature 5 °C to 50 °C are presented here for three recently introduced wavelength / wavenumber Standard Reference Materials (SRM®s): SRM 2035, SRM 2065, and SRM 2036. For all bands in all three SRMs, locations are well described as linear models parameterized with the location at 0 °C (intercept) and the rate of location change per °C (slope). Since these materials were produced from compositionally similar melts, the slopes for each band are identical within measurement imprecision in all three SRMs; only minor differences are observed in the intercepts. Because the direction of change in location differs among the bands, it is possible to use the measured band locations to reliably estimate sample temperature. Two approaches to estimating temperature are evaluated: slope and measurement uncertainty-weighted means. While both methods work well with measurements made under well-characterized and stable environmental conditions, the more complex uncertainty-weighted analysis becomes relatively more predictive as the total measurement uncertainties increase.

INDEXING TERMS

Optical filters

Spectrometer x-axis calibration

Thermometer

Uncertainty-weighted calculations

INTRODUCTION

The National Institute of Standards and Technology (NIST) recently introduced two rare-earth glass optical filter Standard Reference Material®s (SRM®s) suitable for the verification and calibration of the x-axis (as wavenumber, cm^{-1}, or wavelength, nm) of near infrared (NIR) spectrometers operating in transmittance mode. SRM 2035 Near Infrared Transmission Wavelength Standard from 10 300 cm^{-1} to 5130 cm^{-1} was issued in early 1999 (*1, 2*). SRM 2065 UV-Visible, Near-Infrared Transmission Wavelength/Vacuum Wavenumber Standard was issued in early 2002 (*3*). A third glass-based SRM suitable for use with NIR spectrometers operating in diffuse reflectance mode will be available by mid-2003 as SRM 2036. These three optical standards are produced from glass of the same nominal composition and have very similar NIR transmittance properties. Figure 1 displays a representative NIR transmittance spectrum of these materials.

The x-axis locations of the same seven fairly symmetric and well-resolved NIR absorption bands in the three SRMs are certified for a sample temperature of 24 °C ±1.5 °C. Since the location and intensity of NIR absorption features are sensitive to sample temperature (*4 - 6*), the relationships between filter temperature and the x-axis location of each band have been accurately characterized from 5 °C through 50 °C. This enables use of the filters for x-axis calibration at any temperature within this range. It also enables use of the filters as crude thermometers for directly monitoring the temperature of a sample in the spectrometer beam path. The following sections document the temperature-related changes in these seven NIR bands as well as experimental and computational procedures needed to evaluate sample temperature from measured band locations.

MATERIALS, METHODS AND MEASUREMENTS

Glass

The rare-earth glass used for the three NIR wavelength SRMs was of nominal pre-melt composition: 0.106 mass fraction Ho_2O_3, 0.042 mass-fraction Sm_2O_3, 0.025 mass fraction Yb_2O_3, and 0.015 mass fraction Nd_2O_3 in a zirconia-stabilized, borate matrix containing La_2O_3, B_2O_3, and SiO_2. All materials used in the preparation of this glass were of ≥99.8% purity. The glass was prepared by, and purchased from, Schott Glass Technologies (Dureya, Pa).

The three SRMs were prepared from separate melts of this glass. All SRM 2035 filters were prepared from a 1997 melt, all SRM 2065 filters from a 1999 melt, and the glass components of SRM 2036 were prepared from a 2001 melt. These filters were ground and polished at the National Institute of Standards and Technology (NIST) to 25.3 mm ± 0.1 mm in diameter and a thickness of 1.5 mm ±0.1 mm. Each of the SRM 2035 and SRM 2065 units is held in a standard 25.4 mm diameter optical mount (Newport Corporation LH1-100R, Irvine, CA).

NIR Spectrometer

The Bruker IFS66 Fourier Transform (FT) spectrometer (Bruker Optics Inc., Billerica, MA) spectrometer and the x-axis calibration and qualification protocols used in these studies are described in detail elsewhere (*7*). Absorbance versus wavenumber spectra are calculated from interferograms acquired as 256 co-added scans at 4.0 cm^{-1} nominal resolution and zero-filled by a factor of 4 using Opus v3.1 software (Bruker Optics Inc., Billerica, MA). The effective data interval of these spectra is 0.97 cm^{-1}. As determined from analysis of water vapor lines, the observed long-term measurement precision, u_{long}, of this system is 0.03 cm^{-1}.

External sample chamber. All spectra were acquired in a NIST-constructed external sample chamber designed to provide easily modified yet environmentally isolated sample handling. The external sample chamber as well as the spectrometer are purged with dry nitrogen. A

recirculating water bath and several meters of tubing are used to passively control the temperature of the external sample chamber. The temperature of the bath is controlled to 25.0 °C ±0.1 °C.

Single filter studies. A holder for single filters was constructed to fit within the external sample chamber, providing rapid and flexible temperature control of a given filter to within ±0.2 °C from 4 °C through 60 °C. The square aluminum housing of this holder is connected to a dedicated water bath. The housing has two threaded inserts for sample and purge-gas reference measurements. An unmounted filter is sandwiched between two aluminum disks and placed into one of the threaded inserts. A 1.5 cm x 0.75 cm slot cut into both disks serves as the aperture; no beam vignetting is observed. The temperature of the filter is monitored with a thermistor sensor (Omega Engineering Model HH42, with 401 probe, Stamford, CT). The calibration of this sensor is traceable to the NIST Process Measurements Division. This thermistor / digital thermometer combination is accurate to ±0.1°C.

Multiple filter studies. A 33 cm (l) x 23 cm (w) x 25 cm (h) opaque Styrofoam™ inner chamber with open optical ports through its the 2.5 cm thick walls was constructed to surround a six-filter autosampler wheel within the external sample chamber. The same recirculating water bath used with the single filter holder and ≈10 m of polyethylene tubing are used for temperature control. The air temperature within the chamber can be maintained to ±0.3 °C from 15 °C through 52 °C. While requiring 3 h to 4 h to reach thermal equilibrium, this system enables complete temperature profiling of six filters without breaking purge. The temperature of the filters was assumed to be the equilibrium air temperature within the foam container.

Quantitative Measurements

Peak maximum location and absorbance. The maximum absorbance, a_{ij}, for the j^{th} band of the i^{th} spectrum and the x-axis location of the band at this maximum, p_{ij}, are estimated by a five-

point cubic polynomial interpolation to the top of the peak. These estimates are accomplished using the spectrometer's Opus v3.1 software (Bruker Optics Inc., Billerica, MA).

Band 10% height-fraction centroid location. The characteristic x-axis centroid location of the j^{th} absorption band of the i^{th} spectrum is estimated as the 10% height-fraction, b_{ij} (*8*, *9*). The b_{ij} were calculated using a NIST-defined array basic macro in Grams_32 (ThermoGalactic Industries, Salem, NH).

RESULTS AND DISCUSSION

Material Homogeniety

We document elsewhere that for fixed temperatures, the centroid band location variability among the entire SRM 2035 batch is less than 0.03 cm^{-1}; i.e., the location homogeneity of these glasses is equal to or better than the long-term precision of our spectrometric measurements, u_{long} (*10*).

Model Development

In an initial experiment conducted in June 1998, three independent sets of spectra at 10 different temperatures uniformly distributed from ≈5 °C to ≈50 °C were acquired for a single SRM 2035 filter over a period of 2 d. The three sets were acquired at different temperatures using different temperature-change sequences in order to characterize the functional shapes of the relationships while evaluating measurement system stability.

Figure 2 displays the observed relative decrease in maximum peak absorbance, a_{ij}, with increasing temperature for the seven bands. Within measurement uncertainty, all of the absorbance changes for a given filter appear to be linear functions of temperature. No systematic biases were discovered among the data from the three independent sets. While the greatest sensitivity to temperature is for the narrow and intense band 7, there is no strong correlation between the magnitude of the absorbance decline and either the width of the band or the magnitude of its maximum absorbance.

The upper graphical segment of Figure 3 displays the observed relative changes in the peak maximum-based location estimates, p_{ij}. The lower segment of Figure 3 likewise displays the relative changes in the band centroid estimates, b_{ij}. Unlike the consistent decline in a_{ij} with increasing temperature, the location shifts are evenly split between increasing and decreasing wavenumber. The p_{ij} and b_{ij} relationships are qualitatively quite similar; however, the centroid method yields a more precise measure of the temperature behavior of the glass than does the

amplitude peak measurement. The p_{i3} are particularly erratic due to water vapor absorption lines at or near this features absorption maximum (*10*). We only consider the b_{ij} estimates in the following sections of this study.

Measurement Precision

In August 1999, two independent sets of data for a randomly selected SRM 2065 filter along with one set for the same SRM 2035 control filter as used in the 1998 experiment were acquired. The SRM 2035 set consisted of triplicate spectra at nine set temperatures; both 2065 sets consisted of triplicate spectra at eight set temperatures. In May 2001, one independent set of triplicate spectra at nine temperatures was acquired for a randomly selected SRM 2036 filter blank. In all experiments, the filter temperatures were uniformly distributed from ≈5 °C to ≈50 °C. Based upon observation of water-vapor interference in the earlier studies, a longer dry N_2 purge period was employed in the SRM 2036 measurements. In March 2002, data for two SRM 2035, two SRM 2065, and two SRM 2036 filters were acquired using the six-filter autosampler. Six or seven replicate spectra for each of the filters were acquired at four temperatures from 15 °C to 52 °C over a period of 8 d.

The standard uncertainty (aka standard deviation (*11*, *12*)) of the b_{ij} values from each group of replicate spectra estimates short-term measurement precision:

$$u_{k\ell}(b_{ij}) = \sqrt{\sum_{i=1}^{n_{k\ell}} \left(b_{ij} - \bar{b}_j\right)^2 \Big/ \left(n_{k\ell} - 1\right)} \qquad [1]$$

where $\bar{b}_j$ is the mean of the b_{ij} acquired at the ℓ^{th} temperature of the k^{th} study and $n_{k\ell}$ is the number of spectra in that group. In the context of these experiments, these uncertainties include the variation in the measurement and control of filter temperature as well as the estimation of the individual b_{ij} from the acquired spectra. While there is some evidence for increased temperature-control variability at the lowest and highest temperatures, no consistent

relationship between $u_{k\ell}(b_{ij})$ and filter temperature was observed for any of the SRMs (data not shown).

The temperature-specific uncertainties can thus be pooled across all temperatures within each study to provide a temperature-independent standard uncertainty for a given b_{ij}:

$$\overline{u}_k(b_{ij}) = \sqrt{\sum_{i=1}^{n_\ell} u_{k\ell}^2(b_{ij}) \Big/ n_\ell} \qquad [2]$$

where n_ℓ is the number of discrete temperatures evaluated in the given study. While the $\overline{u}_k(b_{ij})$ values for some bands are somewhat different among the studies, the pattern of differences is not consistent across bands or SRMs. We therefore pool the $\overline{u}_k(b_{ij})$ of the different studies in a manner analogous to Equation 2 to estimate the expected measurement uncertainty for a given measurement, $\overline{u}(b_{ij})$. The last two columns of Table 1 list these short-term precision estimates for each band for the single-filter and multiple-filter studies.

With the exception of band 3, the $\overline{u}(b_{ij})$ are similar in magnitude to the spectrometer's long-term measurement precision, 0.03 cm^{-1}. We show elsewhere that the large imprecision for band 3 is a result of water vapor line interference and explore in detail other sources of imprecision in band location measurements (*10*).

Band Location as a Function of Temperature

All b_{ij} measurements from 5 °C through 50 °C are well described by band-specific linear models

$$\hat{b}_{ij} = \alpha_j + \beta_j T_i \qquad [3]$$

where $\hat{b}_{ij}$ denotes the estimated band location, T_i is the temperature in °C of the filter during acquisition of the i^{th} spectra, β_j is the change in band location per °C (temperature coefficient slope) for the j^{th} band, and α_j is the extrapolated location of the band at zero °C (temperature coefficient intercept). The parameters for each band in all studies were estimated by

regression of the replicate average $\bar{b}_j$ on the (unique) filter temperatures. As with the initial data described above, all residuals, $\hat{b}_{ij} - b_{ij}$, were examined graphically for nonlinear behavior. No systematic deviation from the linear model was observed for any band for any of the SRMs.

Figure 4 presents the β_{jk} and α_{jk} temperature coefficients for the most recent single-filter study of each SRM and the March 2002 multi-filter study. These parameters and their standard errors, $u(\beta_{jk})$ and $u(\alpha_{jk})$, are estimated using ordinary least squares regression of the mean observed band locations on the known temperatures. To enable comparison across bands, the parameter values are presented as differences from the mean values, $\bar{\beta}_j$ and $\bar{\alpha}_j$, over all nine studies.

The upper graphical segment of Figure 4 displays the β_{jk} slope deviations. Within measurement uncertainty, the slopes for all three materials are identical. We therefore assign the same temperature coefficient slopes, $\bar{\beta}_j$, to all three SRMs. The combined standard uncertainty of each $\bar{\beta}_j$ is:

$$u_c(\bar{\beta}_j) \cong \sqrt{\frac{u^2(\beta_j) + \bar{u}^2(\beta_j)}{9}} \qquad [4]$$

where the $u(\beta_j)$ are calculated as in Equation 1 (the uncertainty in β for each study) and $\bar{u}(\beta_j)$ as in Equation 2 (the pooled SRM-specific uncertainty).

The lower segment of Figure 4 displays the α_{jk} intercept deviations. While never more than ≈2 cm^{-1} different, the intercepts for the three materials for most bands are quite distinct and therefore cannot be pooled across SRMs. Since intercept and slope estimates are not independent, the α_{jk} for the composite $\bar{\beta}_j$ are recalculated as

$$\alpha_{jk} = \sum_{i=1}^{n_k} \left(b_{ijk} - \overline{\beta}_j T_i \right) \Big/ n_k \qquad [5]$$

where n_k is the number of measurements in the k[th] study. The standard uncertainties for the intercepts of each independent study, $u(\alpha_{jk})$, are estimated as the standard deviation of the $b_{ij} - \overline{\beta}_j T_i$ values in a manner analogous to Equation 1. Each SRM's characteristic intercept, $\overline{\alpha}_{j,SRM}$, is the mean of the α_{jk} of that standard's most recent single-filter study and its two filters in the March 2002 multi-filter study. The combined standard uncertainties, $u_c(\overline{\alpha}_{j,SRM})$, are calculated analogously to Equation 4. Table 1 lists the composite slopes and the SRM-specific intercepts and their associated combined standard uncertainties.

Filter Temperature as a Function of Band Location

Given the $\overline{\beta}_j$ and $\overline{\alpha}_{j,SRM}$ coefficients and their combined standard uncertainties, the filter temperature during spectral acquisition can be estimated from the measured band locations. The estimated filter temperature and associated standard uncertainty using a single b_{ij} is (*13*)

$$\hat{T}_{ij} = \frac{b_{ij} - \overline{\alpha}_{j,\mathrm{SRM}}}{\overline{\beta}_j}\ ;\ u(\hat{T}_{ij}) = \hat{T}_{ij} \sqrt{\frac{u_c^2(\overline{\beta}_j)}{\overline{\beta}_j^2} + \frac{u^2(b_{ij}) + u^2(\overline{\alpha}_{j,\mathrm{SRM}})}{\left(b_{ij} - \overline{\alpha}_{j,\mathrm{SRM}}\right)^2}} \quad . \qquad [6]$$

Since the slopes and measurement variability (Table 1) for the bands are not equal, these individual temperature estimates are unequally influenced by measurement errors. This suggests that the individual estimates should be combined using weights that appropriately adjust the influence of each band (*14*):

$$\overline{T}_i = \frac{\sum_{j=1}^{N} w_j \hat{T}_{ij}}{\sum_{j=1}^{N} w_j}\ ;\ u(\overline{T}_i) = \sqrt{\frac{\sum_{j=1}^{N} w_j \left(\hat{T}_{ij} - \overline{T}_i\right)^2}{(N-1)\sum_{j=1}^{N} w_j}} \qquad [7]$$

where w_j is the weight assigned to the j[th] band and N is the number of bands.

While there are many different possible choices for the weights, two are of most interest. The temperature coefficient slope-based weights

$$w_{j,slope} = \overline{\beta}_j^2 \qquad [8]$$

provide an estimate of filter temperature, $\overline{T}_{i,\text{slope}}$, that gives the minimum root mean-square error (RMSE) for the differences between the observed and predicted band locations:

$$\text{RMSE} = \sqrt{\frac{\sum_{j=1}^{N}\left(b_{ij} - \left(\overline{\alpha}_{j,\text{SRM}} + \overline{\beta}_j \overline{T}_{i,\text{slope}}\right)\right)^2}{N}} \quad . \qquad [9]$$

The measurement uncertainty-based weights

$$w_{j,\text{uncertainty}} = \frac{1}{u_c^2(\hat{T}_{ij})} = \frac{\overline{\beta}_j^4}{u^2(\overline{\beta}_j)\left(b_{ij} - \overline{\alpha}_{j,\text{SRM}}\right)^2 + \overline{\beta}_j^2\left(u^2(\overline{\alpha}_{j,\text{SRM}}) + u^2(b_{ij})\right)} \qquad [10]$$

provide an estimate of temperature, $\overline{T}_{i,\text{uncertainty}}$, that gives the minimum root mean-square uncertainty-normalized error (RMSUNE):

$$\text{RMSUNE} = \sqrt{\frac{\sum_{j=1}^{N}\left(\frac{b_{ij} - (\overline{\alpha}_{j,\text{SRM}} + \overline{\beta}_j \overline{T}_{i,\text{uncertainty}})}{u\left(b_{ij} - (\overline{\alpha}_{j,\text{SRM}} + \overline{\beta}_j \overline{T}_{i,\text{uncertainty}})\right)}\right)^2}{N}} \qquad [11]$$

where $u\left(b_{ij}\text{-}\left(\overline{\alpha}_{j,\text{SRM}} + \overline{\beta}_j \overline{T}_{i,\text{uncertainty}}\right)\right) = \sqrt{\overline{u}^2(b_{ij}) + u^2(\overline{\alpha}_{j,\text{SRM}}) + \frac{u^2(\overline{\beta}_j)}{\overline{T}_{i,\text{uncertainty}}^2}}$ (*13*). Whereas RMSE has the cm^{-1} dimension of the measurements, RMSUNE is in units of the (observed residual) / (expected uncertainty) dimensionless ratio. Figure 5 contrasts RMSE and RMSUNE as functions of temperature for a SRM 2065 exemplar. In all evaluated cases, the RMSUNE potential well for a given set of band locations is slightly narrower than the RMSE well.

To better evaluate the predictive utility of the two methods, 15 new multi-filter set spectra were acquired over a five-day period in April 2002 for each of the same filters studied in March 2002. The $\overline{T}_{i,\text{slope}}$ and $\overline{T}_{i,\text{uncertainty}}$ estimates correlate well (R^2 of 0.997 or better) with the observed filter temperatures and provide similar measurement accuracy, with regard to both

precision (a standard uncertainty of ≈0.5 °C) and bias (from 0 °C to ≈1.5 °C, apparently as a nonlinear function of temperature). The $u(\overline{T}_{i,\text{uncertainty}})$ are smaller and more predictive of the observed precision than are the $u(\overline{T}_{i,\text{slope}})$. Figure 6 displays the differences between predicted and measured temperatures for all six filters.

Figure 6 also displays temperature predictions for the initial 1998 SRM 2035 single-filter study. While these estimates are on average unbiased, the precision is much poorer than for the "modern" multi-filter study. The combined uncertainties for both temperature estimates are much larger than the observed precisions. This suggests that the filter temperatures in this early experiment were less well determined and less stable during spectral acquisition than originally believed. The superior precision provided by $\overline{T}_{i,\text{uncertainty}}$ (a standard uncertainty of ≈1.2 °C rather than ≈2.2 °C) for these data suggests that the more complex uncertainty weights of Equation 10 become more useful as measurements become less certain.

DISCLAIMER

Certain commercial materials, instruments, software, and equipment are identified in this paper to specify the experimental procedure as completely as possible. In no case does such identification imply a recommendation or endorsement by the National Institute of Standards and Technology, nor does it imply that the material, instrument, software, or equipment is necessarily the best available for the purpose.

ACKNOWLEDGMENTS

We thank Katherine E. Sharpless for her constructive criticism and patient guidance towards better clarity and structure for this and related reports.

REFERENCES

1 SRM 2035 Certificate, National Institute of Standards and Technology, "Standard Reference Material 2035 Near Infrared Transmission Wavelength Standard from 10300 cm^{-1} to 5130 cm^{-1}",Standard Reference Materials Program, NIST, Gaithersburg, MD 20899, 22 February 1999. http://srmcatalog.nist.gov/nist/products.nsf/certs/2035?OpenDocument

2 Choquette, S. J.; Travis, J. C.; O'Neal, L. E.; Zhu, C.; Duewer, D. L. Spectroscopy **2001,***16*(4), 14-19.

3 SRM 2065 Certificate, National Institute of Standards and Technology, "Standard Reference Material 2065 Ultraviolet-Visible-Near-Infrared Transmission Wavelength/Vacuum Standard", Standard Reference Materials Program, NIST, Gaithersburg, MD 20899, 28 March 2002. http://srmcatalog.nist.gov/nist/products.nsf/certs/2065?OpenDocument

4 Wülfert, F.; Kok, W. Th.; Smilde, A. G. Anal. Chem. **1998**, *70*(9), 1761-1767.

5 Lin, J. Appl. Spectrosc. **1998**, *52*(12), 1591-1596.

6 Wülfert, F.; Kok, W. Th.; de Noord, O. E.; Smilde, A. G. Anal. Chem. **2000**, *72*(7), 1639-1644.

7 Choquette, S.J., O'Neal, L.E., Duewer, D.L. Hannsen, L.M, Zhu, C. *This currently is "Available from the author" as a NIST-approved submission; it will soon be submitted to Applied Spectroscopy.*

8 Cameron, D.G., Kauppinen, J.K., Moffat D.J., Mantsch H.H. *Appl. Spectrosc*. 1982, 36, 245-250.

9 ASTM Committee E-13. "E1421-99: Standard Practice for Describing and Measuring Performance of Fourier Transform Mid-Infrared (FT-MIR) Spectrometers Level Zero and Level One Tests", ASTM, 100 Barr Harbor Drive, PO Box C700, West Conshohocken, PA 19428-2959, 1999.

10 Choquette, S.J., O'Neal, L.E., Duewer, D.L., and Filliben, J.J. *This currently is "Available from the author" as a NIST-approved submission; it has been submitted to Anal Chim Acta.*

11 International Organization for Standardization (ISO), Guide to the Expression of Uncertainty in Measurement, ISO, Geneva, Switzerland, 1995.

12 Taylor, B.N., Kuyatt, C.E. Guidelines for evaluating and Expressing Uncertainty in NIST Measurement Results, NIST Technical Note 1297, NIST, Gaithersburg, MD (1994). http://www.physics.nist.gov/cuu/Uncertainty/bibliography.html

13 Bevington. P.R., Robinson, D.K. Data Reduction and Error Analysis for the Physical Sciences, 2nd Ed. WCB McGraw Hill, Boston, MA (1992).

14 DATAPLOT Reference Manual available online at: http://www.itl.nist.gov/div898/software/dataplot.html/homepage.html

Table 1. Parameters and Uncertainties for 4 cm^{-1} Resolution Spectra

		$\bar{\alpha}_{j,SRM}$, cm^{-1} [b]			$\bar{u}(b_{ij})$, cm^{-1}	
Band	$\bar{\beta}_j$, $cm^{-1}/°C$ [a]	SRM 2035	SRM 2065	SRM 2036	Single [c]	Multi [d]
1	-0.0494(15)	5139.90(4)	5140.63(7)	5139.77(12)	0.039	0.012
2	0.0878(16)	6802.61(6)	6804.17(8)	6802.16(5)	0.050	0.040
3	0.012(6)	7312.9(3)	7314.5(4)	7312.41(12)	0.37	0.074
4	0.0597(10)	8177.10(5)	8178.50(6)	8176.78(6)	0.042	0.029
5	-0.0395(15)	8682.75(7)	8683.61(9)	8682.5(2)	0.064	0.078
6	-0.0751(19)	9296.08(11)	9296.5(2)	9295.84(15)	0.052	0.078
7	0.0179(7)	10245.16(6)	10245.24(5)	10245.12(3)	0.029	0.028

a) Average temperature coefficient slopes for all three optical standards. The digits in parentheses denote the combined standard uncertainty in units of the last reported digit of the slope.

b) Average temperature coefficient 0 °C intercepts for each of the three optical standards. The digits in parentheses denote the combined standard uncertainty in units of the last reported digit of the intercept.

c) Expected short-term precision of b_{ij} measurements made using the single-filter holder and the 1998-2001 operating protocol.

d) Expected short-term precision of b_{ij} measurements made using the multiple-filter holder, secondary temperature control chamber, and the 2002 operating protocol.

FIGURE CAPTIONS

Figure 1. Representative FT-NIR spectrum of zirconia-stabilized, borate matrix glass of nominal rare-earth composition: 0.106 mass fraction Ho_2O_3, 0.042 mass-fraction Sm_2O_3, 0.025 mass fraction Yb_2O_3 and 0.015 mass fraction Nd_2O_3. The bands with certified x-axis location are designated with the digits 1 through 7.

Figure 2. Absorbance vs temperature. The change in maximum absorbance, a_{ij}, for the seven bands as functions of filter temperature relative to the extrapolated absorbances at 0 °C. For graphical clarity, open circles denote the a_{i3} and open squares denote the a_{i6}; the a_{ij} for the other five bands are denoted as the band index digit. The lines denote least squares fits of a linear model to each band.

Figure 3. Peak and band location vs temperature. The upper segment displays the change in peak locations, p_{ij}, for the seven bands as functions of filter temperature, relative to their extrapolated locations at 0 °C. The lower segment displays changes in the band centroid locations, b_{ij}. The lines denote unweighted least squares fits of a linear model to each band.

Figure 4. Deviations of linear model slopes (β_j) and intercepts (α_j) for the three optical standards. The upper segment displays the differences between the individual β_j and their all-experiment means. The open diamonds denote SRM 2035 values, the solid circles denote SRM 2065, and the open squares denote SRM 2036. The error bars span ±2 standard error estimates on the parameter. The lower segment likewise displays the differences between the individual α_j and their all-experiment means.

Figure 5. Representative potential wells for slope- and uncertainty-weighted temperature estimation. The light curve traces the slope-weighted RMSE well of Equation 9 as a

function of trial-temperature for a SRM 2065 exemplar spectrum, acquired at a nominal temperature of 11.5 °C; the dark curve likewise traces the uncertainty-weighted RMSUNE well of Equation 11. The solid and open circles denote the predicted temperatures from the two calculations; the chords across the wells represent ± one combined standard uncertainty about the predicted temperatures.

Figure 6. Predicted slope- and uncertainty-weighted temperatures. The left segment displays differences between slope-weighted predictions and measured temperatures; the right segment likewise displays the differences for uncertainty-weighted predictions. The six filters of the April 2002 multi-filter set are denoted as open and solid symbols: circles for SRM 2035, squares for SRM 2036, and triangles for SRM 2065. The June 1998 SRM 2035 single-filter predictions are denoted "×". For graphical convenience, the error bars span approximate 40% confidence intervals about the predicted temperatures.

Figure 1

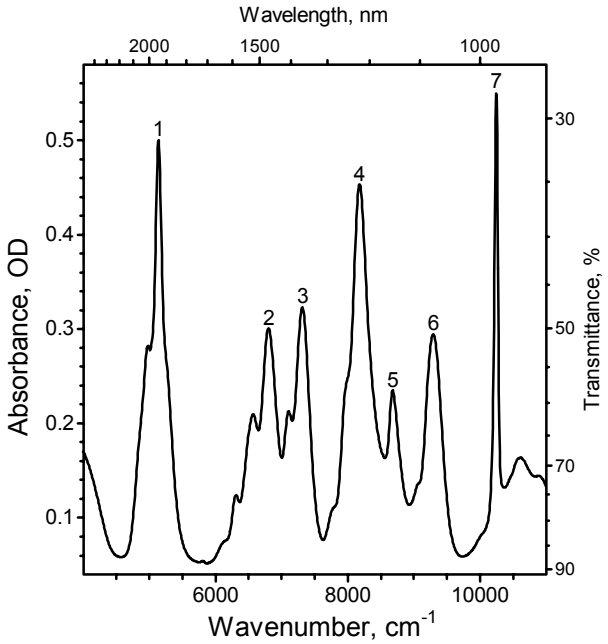
Wavelength, nm
2000
1500
1000
1
2
3
4
5
6
7
0.5
0.4
0.3
0.2
0.1
Absorbance, OD
30
50
70
90
Transmittance, %
6000
8000
10000
Wavenumber, cm-1

Figure 2

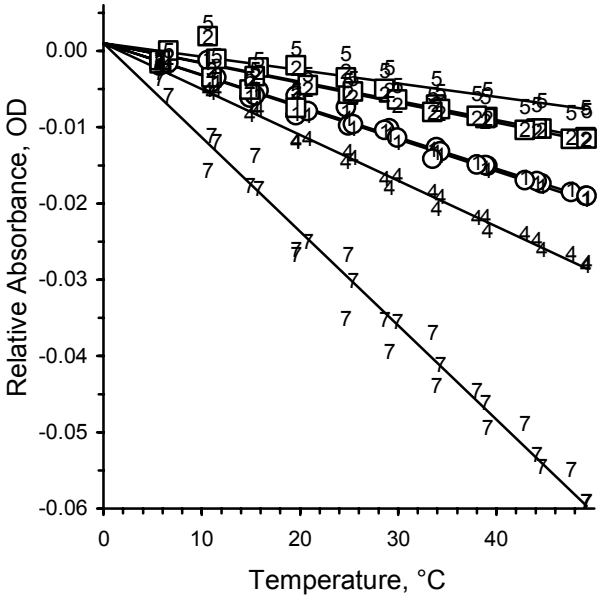
Relative Absorbance, OD
0.00
-0.01
-0.02
-0.03
-0.04
-0.05
-0.06
0
10
20
30
40
Temperature, °C

Figure 3

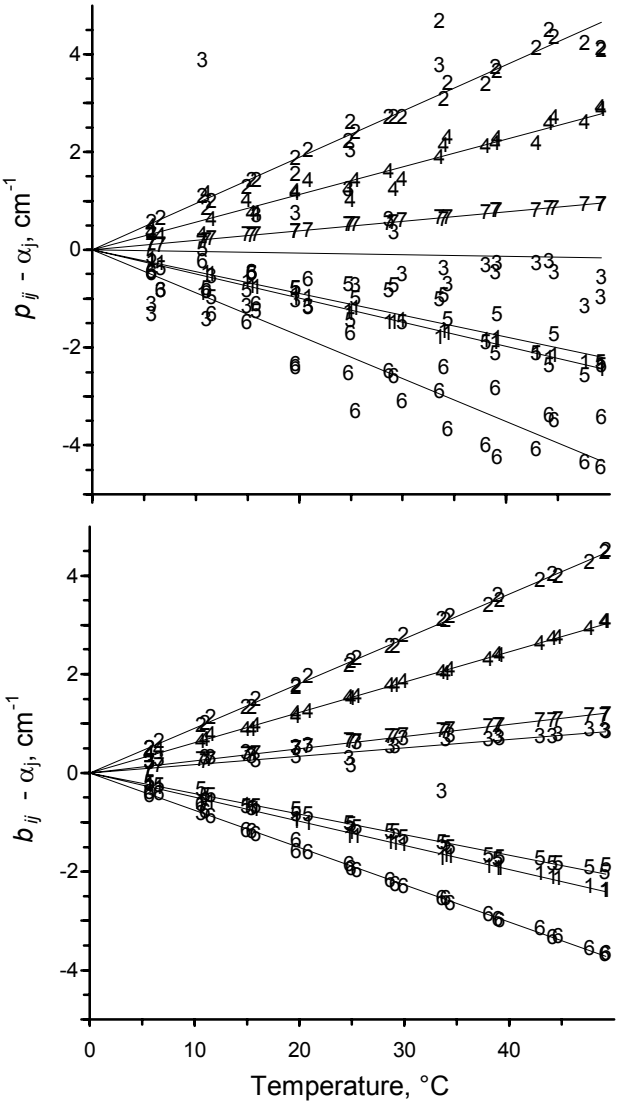
p_{ij} - α_j, cm^{-1}
b_{ij} - α_j, cm^{-1}
Temperature, °C
0
10
20
30
40
4
2
0
-2
-4

Figure 4

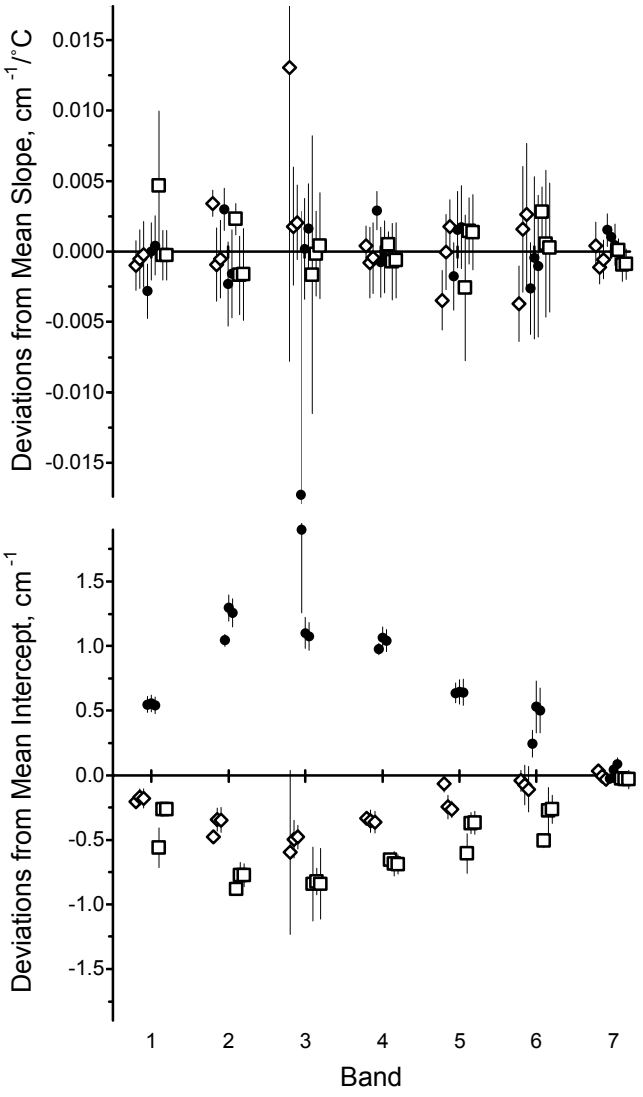
Deviations from Mean Slope, cm -1/°C
0.015
0.010
0.005
0.000
-0.005
-0.010
-0.015
Deviations from Mean Intercept, cm -1
1.5
1.0
0.5
0.0
-0.5
-1.0
-1.5
1
2
3
4
5
6
7
Band

Figure 5

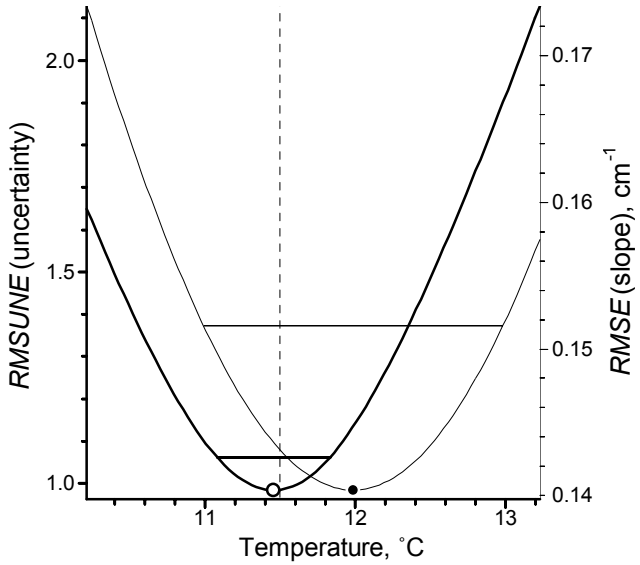
2.0
1.5
1.0
RMSUNE (uncertainty)
0.17
0.16
0.15
0.14
RMSE (slope), cm-1
11
12
13
Temperature, ˚C

Figure 6

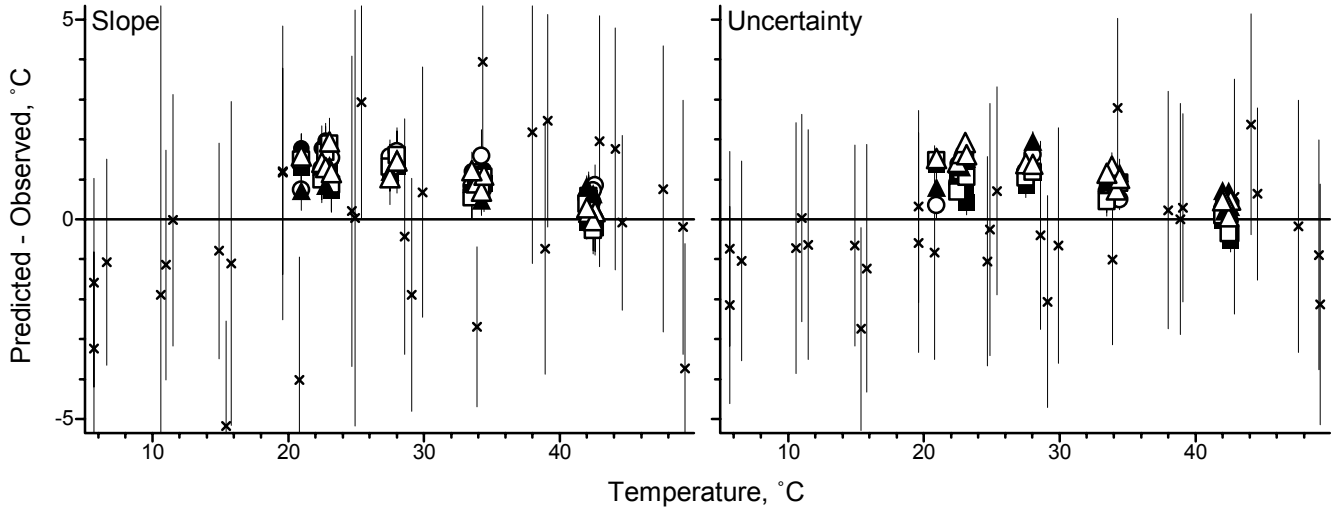
Slope
Uncertainty
Predicted - Observed, ˚C
Temperature, ˚C
5
0
-5
10
20
30
40